EXTRACTING METAL AND EDGE RECOMBINATION PARAMETERS WHICH ARE COMPATIBLE WITH MULTI-DIMENSIONAL CELL SIMULATIONS

Pierre Saint-Cast, David Herrmann, Puzant Baliozian, Hannah Stolzenburg, Hannes Hoeffler, Andreas Fell

Fraunhofer Institute for Solar Energy Systems ISE, Heidenhofstraße 2, 79110 Freiburg, Germany

ABSTRACT: In this work, an analytical model is presented that reproduces lateral changes in *pn*-junction voltage as a result of recombination at linear shaped defect. The model takes into account the majority charge carrier transport in the emitter and in the base as induced by a metal finger, an edge or any linear region with a high local recombination rate. It predicts the *pn*-junction voltage as a function of distance to the perturbation in one dimension. A comparison of the model with numerical device simulations using Quokka3 shows low deviation for the local voltage under the finger (< 2 mV) and at the edge (< 5 mV).

The presented method to interpret the photoluminescence image of a wafer with a metal front grid is based on Fourier analysis. For each saturation current density at the metal, we can associate a predicted Fourier peak set obtained from the model. The saturation current density at the metal finger is obtained when the peaks of the photoluminescence image and the model correspond best. The model is also applied to the interpretation of photoluminescence images in the aim of evaluating the local saturation current density at the edge. In this case, photoluminescence images of the wafer edges are carried out at different illumination intensities. The *pn*-junction voltage profile towards the edge is calculated from the photoluminescence image of the wafer. For each illumination intensity, the saturation current density at the edge is obtained by adjusting the parameter of the model to the photoluminescence image. Finally, we obtain the saturation current density at the edge as a function of the carrier injection.

Keywords: Analytical model, Photoluminescence image, Metal recombination, Edge recombination.

1 INTRODUCTION

1.1 Context

Recombination under the emitter contacts (on the front surface) has been a subject of study for a long time [1, 2] in the field of photovoltaics. The same can be said for recombination at the edges of the cell [3]. The first subject is still very relevant, as the front contact recombination represents a major loss for state-of-the-art solar cells [4]. High-efficiency modules, featuring half cells, quarter cells or shingled cells, are developing rapidly. Decreasing the size of the cell leads to an increase of the perimeter-to-cell area ratio, that hence an increase of the second diode-like losses occur on the edges [5]. The question of quantifying both recombination types is the focus of this paper.

Despite the increasing use of numerical simulations in the photovoltaic (PV) community for solar cell device modelling [6–8], the interpretation of characterization results are still mostly analyzed using simple analytical models. For example, in most cases [9–11], the recombination under the front contacts is modelled by a constant *pn*-junction voltage model. In this case, the effective saturation current density ($j_{0\text{eff}}$) only depends on the saturation current density without metal j_0, on the saturation current density on the metal $j_{0\text{met}}$ and on the metal area fraction F_{met} following

$$j_{0\text{eff}} = (1 - F_{\text{met}}) j_0 + F_{\text{met}} j_{0\text{met}} . \tag{1}$$

The value of $j_{0\text{met}}$ obtained by this method might be used in a PC1D [12] solar cell model, but not in multi-dimensional models like Quokka and Sentaurus [6–8]. As Herrmann et al. [13] have shown recently, the interpretation of the same experimental results using Quokka leads to significantly different $j_{0\text{met}}$ values compared to the results using a constant *pn*-junction voltage model.

A model corresponds to a certain interpretation of the reality; in order to do a simulation of a phenomenon, we obviously need a model. While less obvious and often not stated specifically in publications, the interpretation of a measurement also needs a model. When presented like this, it follows that the model for the simulation and for the measurement interpretation should be the same, or at least compatible. Unfortunately, this simple but fundamental methodological rule is not always respected.

For measurement purposes, the use of simple models is often preferred. However for simulation, the use of the most accurate model will be beneficial. Our approach tries to balance relative simplicity with accuracy.

1.2 Approach

In this contribution, we first present an analytical model [14] of charge carrier transport in the cases of front metal recombination and edge recombination. The compatibility of this model compared with multi-dimensional simulations (Quokka) is verified.

Then, two different characterization methods (based on this model) are developed. The idea is to extract a map of the *pn*-junction voltage (*V*) from a calibrated photoluminescence imaging (PLi). Finally, the measured *V*(x) profile as a function of the position is compared to the analytical model to extract the recombination parameters under the metal fingers [15] or at the edges [16] of the solar cell.

2 MODEL CONSTRUCTION

Both, recombination under front metal fingers and recombination at the edges can be included into the category of linear recombination centres close to or at the *pn*-junction. This is in contrast to local recombination on the rear surface (e.g. rear contact recombination), where the recombination is mainly limited by the diffusion of minority carriers. Specifically, we focus on the recombination under a finger, busbar, scratch on the front surface or at the edge of the solar cell. By assuming that translation along the axis of the defect in the system does not vary, we can reduce the dimension to a two-dimensional system. We suppose that the linear defect is the only source of inhomogeneity in our system.

Everywhere else in the system, there is generated current j_{lum} and saturation current density j_0 (which combines the emitter, bulk and rear recombination together). The high recombination rate at the defect (compared to the rest of the cell) induces a lower *pn*-junction potential difference (or a lower excess carrier density) in its proximity. This local depletion of potentials leads to a flow of electrons and holes towards the defect.

Therefore, it is clear that this problem will be a carrier transport problem. In this model we suppose (hypothesis 1) that over relevant distances (> 1 mm) to the size of the device (> 1 cm) the lateral carriers flow will be limited by resistive losses. In order to simplify this problem further we suppose (hypothesis 2) that the vertical transport effects in the emitter and the bulk are small compared to lateral transport and can be modelled by a sheet resistance (ρ_e and ρ_b respectively). The problem is now one dimensional with an emitter region and a bulk region. The origin of the x axis is defined to be the location of the linear defect. The local electrostatic potential in the emitter region is $V_e(x)$, and the local potential in the bulk region is $V_b(x)$. Therefore, the local potential difference at the *pn*-junction is $V(x) = V_e(x) - V_b(x)$. In figure 1, a schematic of the problem in 3 dimensions is shown and compared to the model developed. The model mentioned below corresponds to the solution of the continuity equation considering only resistive carrier transport and recombination. It is not the purpose of this abstract to have a complete demonstration of this model. The set of equations will be presented in a peer-reviewed article in a scientific journal [14]. In the following section the results of the model will be presented.
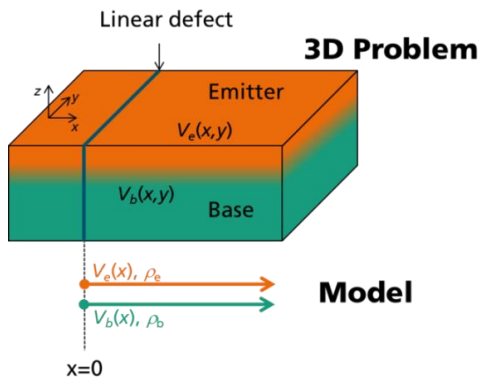
Figure 1: Schematic of the problem in 3 dimensions compared to a simplified interpretation which corresponds to the model proposed in this paper. Figure extracted from [14].

3   APPLICATION OF MODEL

3.1 Characterization of the recombination under a contact

The contacts on the front surface are long and thin, so their geometry can be described as linear (w is the contact width and p the spatial period or pitch). The contacts are parallel to each other. In the absence of any contacts, the voltage (implied open-circuit voltage iV_{OC}) difference at the *pn*-junction would be homogeneous. Due to the additional recombination at the contacts, the voltage maximum V_{max} is lower than iV_{OC}. V_{max} will be obtained between two contacts (middle position).

In figure 2, the potential difference at the *pn*-junction V is shown as a function of the position for an exemplary cell

(where $iV_{OC} = 680$ mV, $\rho_{eff} = 180$ Ω/sq, $j_{lum} = 40$ mA/cm², $w = 50$ µm and $p = 1400$ µm). The saturation current density under the contact (j_{0met}) is varied from $j_{0met} = 500$ fA/cm² to $j_{0met} = 10$ pA/cm². The analytical model developed is compared to Quokka simulation; a very good agreement of about ±1 mV is obtained in the entire range of parameters tested. We have just shown the compatibility between our model and Quokka simulation. In the next section we will use the model to analyze the voltage profile between fingers in order to extract the j_{0met} value.
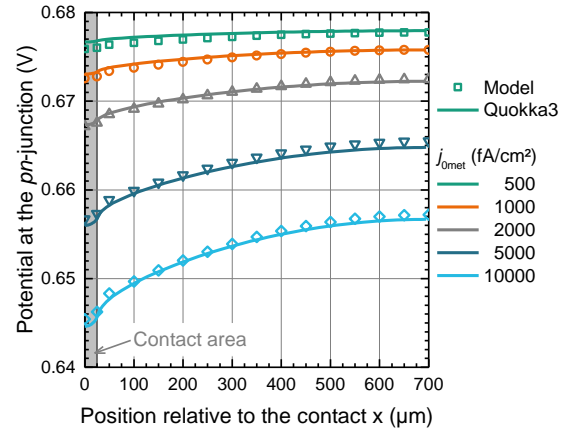
Figure 2: Potential difference at the pn-junction as a function of distance to the contact for the different j_{0met}. The fixed parameters are $j_{lum} = 40$ mA/cm², $iV_{OC} = 680$ mV, $\rho_{eff} = \rho_e + \rho_b = 180$ Ω/sq, $w = 50$ µm and $p = 1400$ µm. Figure extracted from [14].

Calibrated photoluminescence imaging is used to obtain *pn*-junction voltage maps. Short-pass filters (in our case from a wavelength of 1000 nm) guarantee that most of the light comes from the front surface of the wafer, close to the *pn*-junction. In figure 3, an example of a PL image of a test sample with a front *pn*-junction, a front Ag contact grid, and front and rear passivation is shown. In figure 5 (top), the voltage profile obtained for a part of the PL image in figure 3 is shown. At each finger, there is a *pn*-junction voltage minimum, which increases slowly, reaching a maximum between the fingers. This regular behaviour overlaps another chaotic, slower evolution of *pn*-junction voltage. The latter corresponds to the wafer local defects and process inhomogeneities, both of which affect the lifetime.

Figure 3: Photoluminescence image signal of a section of the test sample. Figure extracted from [15].

Fitting each profile between fingers independently is a time intensive process. In addition, there are two major problems. First, the inhomogeneity of the lifetime will produce multiple results. This makes it difficult to find relevant values. Second, the size of the pixel is about 3 times the size of the finger. Therefore the finger positions need to be defined in a sub pixel range for all fingers, which is very complicated. For these reasons, we have chosen another approach based on the fact that the front

grid is periodic. The analysis of the Fourier spectra offers the possibility to isolate only the signal change due to the fingers (finger frequency and harmonic), which eliminates the problem of wafer homogeneity. Numerical data can be efficiently converted in Fourier spectrum using the fast Fourier algorithm. In figure 4 (green curve), the Fourier spectrum corresponding to the PL image in figure 3 is plotted. The Fourier spectrum is also voltage calibrated. The middle peak corresponds to the average *pn*-junction voltage. The other peaks correspond to the first, second, third and fourth harmonics, from left to right, for positive frequencies and from right to left for negative frequencies. We notice that the peaks are perfectly symmetric.
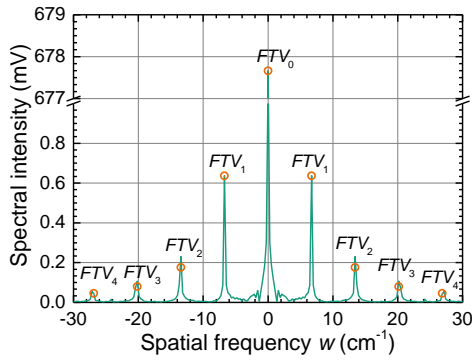
Figure 4: Fourier spectra corresponding to the *pn*-junction voltage profile (green curve), Fourier spectra corresponding to the analytical model (orange points). Figure extracted from [15].
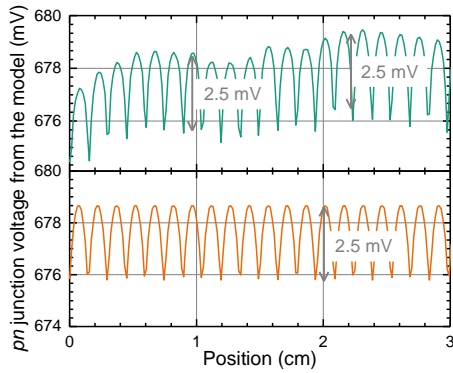
Figure 5: Top: Sample of the *pn*-junction voltage map (voltage calibrated PL image). Bottom: Sample of the Fourier inverse of the spectra of the fitted analytical model. Figure extracted from [15].

For the analytical model, theoretical Fourier spectra can be calculated as well. In this case it is a Fourier series. We call a member of the series FTV_n, where n is the index in the series. The index 0 corresponds to the middle peak in the spectra, the index 1, 2, etc. correspond to the first, second, etc. harmonics, respectively. In figure 4 (orange points), the Fourier spectra based on the model is plotted. Only the peaks are visible. As expected, the spectrum is 0 between the peaks. The model parameters are adjusted until that FTV_0 and FTV_1 correspond to the measured values. FTV_2, FTV_3, FTV_4 are model predictions. It is expected that higher harmonics are more difficult to fit, as image blurring preferentially affects high frequencies.

A Fourier spectrum can be transformed back to the

original image using a Fourier inverse algorithm. The orange curve in figure 5 corresponds to the Fourier inverse of the theoretical spectrum. As the spectrum is truncated, the signal obtained is also pixelated with the same pixel density as the measurement. The signal of the model is very similar to the measurement but without the inhomogeneity of the wafer.

Finally, we need to extract the values (iV_{OC} and j_{0met}) we are looking for. These cannot be obtained directly. Therefore a lookup table needs to be built (see Figure 6). Two unknown input parameters (iV_{OC}, V_{max}) are varied, the corresponding j_{0met}, FTV_0 and FTV_1 are obtained by applying the model. Each result is reported in a table. For FTV_0 and FTV_1 values calculated from the PL measurement, the corresponding iV_{OC} and j_{0met} are taken from the lookup table.
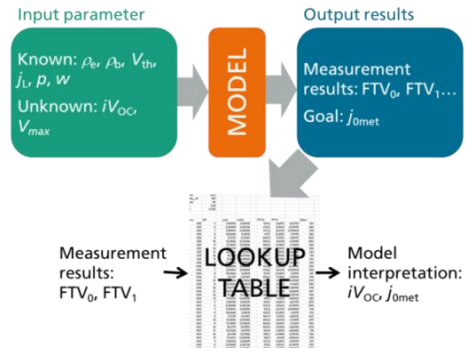
Figure 6: Procedure needed to analyze the characterization results and extract the iV_{OC} and the j_{0met} values. Figure extracted from [15].

3.2 Application of the model to edge recombination

In the proposed model, we only consider one edge in an infinite wafer. Under open-circuit conditions, the *pn*-junction voltage decreases toward the edge due to recombination at the edge. In figure 7, the *pn*-junction voltage is plotted as a function of the position for six different illumination intensities. For low illuminations, the *pn*-junction voltage is affected by the edge over a much greater distance than for high illumination. The results of the models are compared to Quokka simulations, and are found to be in good agreement within a deviation of ± 3 mV.
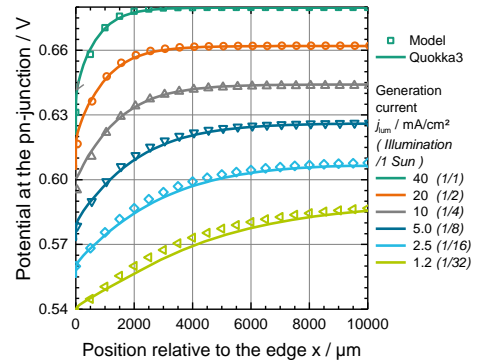
Figure 7: Potential difference at the *pn*-junction as a function of distance to the edge for different illumination intensities with $iV_{OC} = 680$ mV, $\rho_{eff} = 180$ Ω/sq and $j_{02edge} = 19$ nA/cm. Figure extracted from [14].

For this example, the recombination parameter at the edge is $j_{02edge} = 19$ nA/cm, which corresponds to a "worst-case" value as identified by Fell *et al.* [17].

In order to quantify the recombination at the edge, calibrated PL imaging is carried out on *n*-type iV_{OC} test samples. The wafers used were shiny etched float zone Si with a front boron emitter passivated by an Al_2O_3 / SiN_X layer stack and rear-side SiN_X passivation. The wafer is cleaved through the *pn*-junction by means of thermal laser separation (TLS) [18]. The potential at the *pn*-junction is measured by means of calibrated PL measurements for six illumination intensities. In figure 8, the potential profile towards the edge is plotted as a function of position relative to the edge. The experimental results are compared to the model. For each illumination intensity, the recombination parameter at the edge is adjusted. The analytical model does not limit the choice of the edge recombination model. Any function linking the recombination current and the *pn*-junction potential at the edge can be used a priori. Therefore the method proposed allows of the evaluation of the edge recombination as a function of the carrier injection. To each illumination intensity in figure 8 corresponds to an injection level.
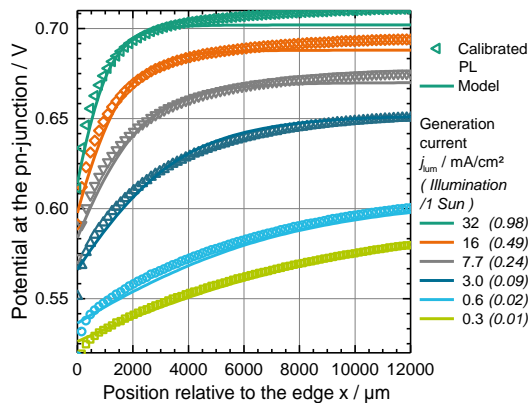
Figure 8: Potential difference at the *pn*-junction as a function of distance to the edge measured by calibrated PL measurement for different illumination intensities.

4 SUMMARY

The developed analytical model [14] is shown to be compatible with Quokka simulation for modeling the recombination under the front metal grid and for edge recombination. The possibilities presented by this model are used to develop two characterizations methods:

The first method [15] allows the extraction of the recombination under the metal grid by analyzing the PL image of a metalized sample in the Fourier space. This method does not require a variation of the metal fraction. By analyzing separately the PL mean signal and its variation between the fingers, j_{0met} and the iV_{OC} can be extracted from a single image.

The second method [16] allows the characterization of the recombination at the edge by analyzing how the *pn*-junction signal decreases towards the edge. The analysis is based on calibrated PL images with different illumination intensities. As a result, the recombination at the edge is extracted as a function of the carrier injection.

5 ACKNOWLEDGEMENTS

6 REFERENCES

[1] A. Cuevas and S. López-Romero, "The combined effect of non-uniform illumination and series resistance on the open-circuit voltage of solar cells," *Solar Cells*, vol. 11, no. 2, pp. 163–173, 1984.

[2] R. R. King, R. A. Sinton, and R. M. Swanson, "Studies of diffused phosphorus emitters: Saturation current, surface recombination velocity, and quantum efficiency," *IEEE Trans. Electron Devices*, vol. 37, no. 2, pp. 365–371, 1990.

[3] K. R. McIntosh, "Lumps, humps and bumps: three detrimental effects in the current-voltage curve of silicon solar cells," PhD thesis, University of New South Wales, Sydney, Australia, 2001.

[4] P. Saint-Cast, S. Werner, J. Greulich, U. Jäger, E. Lohmüller, and R. Preu, "Analysis of the losses of industrial-type PERC solar cells," *Phys. Status Solidi RRL*, 2016.

[5] S. W. Glunz, J. Dicker, M. Esterle, M. Hermle, J. Isenberg, F. J. Kamerewerd, J. Knobloch, D. Kray, A. Leimenstoll, F. Lutz, D. Oßwald, R. Preu, S. Rein, E. Schäffer, C. Schetter, H. Schmidhuber, H. Schmidt, M. Steuder, C. Vorgrimler, and G. Willeke, "High-efficiency silicon solar cells for low-illumination applications," in *29th IEEE Photovoltaic Specialists Conference New Orleans*, New Orleans, 2002, pp. 450–453.

[6] Synopsys TCAD, *Sentaurus Device*: Synopsys, 2013.

[7] A. Fell, "A free and fast three-dimensional/two-dimensional solar cell simulator featuring conductive boundary and quasi-neutrality approximations," *IEEE Trans. Electron Devices*, vol. 60, no. 2, pp. 733–738, 2013.

[8] A. Fell, J. Schön, M. C. Schubert, and S. W. Glunz, "The concept of skins for silicon solar cell modeling," *Sol. Energy Mater. Sol. Cells*, vol. 173, pp. 128–133, 2017.

[9] T. Fellmeth, A. Born, A. Kimmerle, F. Clement, D. Biro, and R. Preu, "Recombination at metal-emitter interfaces of front contact technologies for highly efficient silicon solar cells," *Energy Proced.*, vol. 8, pp. 115–121, 2011.

[10] A. Edler, V. D. Mihailetchi, L. J. Koduvelikulathu, C. Comparotto, R. Kopecek, and R. Harney, "Metallization-induced recombination losses of bifacial silicon solar cells," *Prog. Photovolt: Res. Appl.*, n/a, 2014.

[11] S. Werner, E. Lohmüller, A. Wolf, and F. Clement, "Extending the limits of screen-printed metallization of phosphorus- and boron-doped surfaces," *Sol. Energy Mater. Sol. Cells*, 2016.

[12] D. A. Clugston and P. A. Basore, "Modelling free-carrier absorption in solar cells," *Prog. Photovolt: Res. Appl.*, vol. 5, no. 4, pp. 229–236, 1997.

[13] D. Herrmann, S. Lohmüller, H. Höffler, A. Fell, A. A. Brand, and A. Wolf, "Numerical Simulations of Photoluminescence for the Precise Determination of Emitter Contact Recombination Parameters," *IEEE J. Photovoltaics*, (Accepted for publication).

[14] P. Saint-Cast and A. Fell, "An Analytical Model for Resistance-Limited Recombination at Line

Defects in Solar Cells," *IEEE J. Photovoltaics*, p. 1, 2019.

[15] P. Saint-Cast, D. Hermann, and H. Höfler, "Information on recombination under front fingers based on Fourier analysis of photoluminescence images," *Submitted*.

[16] P. Saint-Cast and et al., *To be published*.

[17] A. Fell, J. Schön, M. Müller, N. Wöhrle, M. C. Schubert, and S. W. Glunz, "Modeling Edge Recombination in Silicon Solar Cells," *IEEE J. Photovoltaics*, pp. 1–7, 2018.

[18] S. Eiternick, F. Kaule, H.-U. Zühlke, T. Kießling, M. Grimm, S. Schoenfelder, and M. Turek, "High Quality Half-cell Processing Using Thermal Laser Separation," *Energy Procedia*, vol. 77, pp. 340–345, 2015.